

---

# When Think-with-Image Meets Safety: What Determines Multimodal Jailbreak Robustness?

---

**Yuan Tian\***

Independent Researcher

**Bing Hu\***

Independent Researcher

**Fang Wu**

Stanford University

**Xiaomin Li**

Harvard University

**Binghang Lu**

Purdue University

**Neil Zhenqiang Gong**

Duke University

## Abstract

Think-with-image reasoning is emerging as a new inference paradigm for large vision-language models, but its safety implications remain poorly understood. Existing systems already span multiple process designs, including direct response generation, text-only prior turn, visual-state manipulation, and explicit external image-tool invocation. In this paper, we ask which of these evaluated paradigms improves multimodal jailbreak robustness, and why. Across multiple vision-language models, explicit image-tool interaction yields the lowest attack success rates in our experiments, reducing jailbreak success by around 30% relative on average across the evaluated models. This finding is initially surprising: ASR remains low even when the returned image-tool output is manually overridden or itself unsafe-looking, but returns near direct-answering levels under text-only prior turn controls. These results indicate that the lower ASR is not explained by benign returned-image semantics or by the textual image-tool trace alone. To explain the pattern, we introduce an *image-tool safety vector* framework that models image-tool invocation as a residual shift in hidden representations toward a safety-relevant direction. Representation-level analyses and activation interventions support this account. Overall, our results suggest that explicit image-tool interaction is a promising design pattern for improving jailbreak robustness, while also motivating pipeline-specific safety evaluation.

## 1 Introduction

Large vision-language models (LVLMs) are rapidly moving from single-pass image-text inference toward *think-with-image* (TwI) reasoning, where natural-language reasoning is interleaved with intermediate visual operations [Wu et al., 2023, Surís et al., 2023, Yang et al., 2023b, Wu and Xie, 2024, Su et al., 2025a]. Existing systems span paradigms ranging from direct image generation or editing to grounding intermediate steps to regions, sketches, or coordinates [Yang et al., 2023a, Peng et al., 2023, Gupta and Kembhavi, 2023], and frameworks such as Visual Sketchpad [Hu et al., 2024] and Chain of Multi-modal Thought [Cheng et al., 2025b] further augment LVLMs with external tools, including object detectors, segmenters, and geometric solvers, whose outputs are fed back into later reasoning [Yao et al., 2023, Schick et al., 2023, Lu et al., 2023, Chen et al., 2026]. This shift has

---

\*Equal contribution.

†Corresponding authors: yuan.tian.research@gmail.com, binghuresearch@gmail.com.

expanded multimodal capability on tasks requiring spatial grounding, compositional perception, and multi-step decision making.

However, think-with-image reasoning is not only a capability shift; it is also a structural change to the inference process. Different paradigms introduce different intermediate states, control flows, and external interactions. Compared with direct query-response generation, image-tool-augmented interleaving inserts additional decision points: the model decides whether to call an image tool, produces a structured image-tool request, consumes a returned visual artifact, and conditions later reasoning on that artifact. These interaction steps introduce token patterns and visual states that are absent from standard end-to-end inference. As a result, the safety behavior of a TwI system cannot be inferred directly from the safety properties of the base model alone, and different paradigms may have materially different safety profiles.

This question is increasingly important as multimodal systems are deployed in settings where visual reasoning and tool use are closely intertwined [Zheng et al., 2024, Xie et al., 2024, Koh et al., 2024]. Prior work shows that LVLMs remain vulnerable to harmful image-text inputs [Liu et al., 2024, Luo et al., 2024], while tool-use safety studies have mainly examined text-only agents or risks introduced by external tools [Greshake et al., 2023, Ruan et al., 2024, Zhan et al., 2024, Debenedetti et al., 2024]. Yet it remains unclear how different TwI paradigms affect safety behavior: explicit image-tool interaction may amplify multimodal jailbreak risk, shift failure modes, or even improve robustness.

We study this question across multiple TwI paradigms and vision-language models, with a particular focus on explicit image-tool invocation. Our main empirical finding is counterintuitive: **explicit image-tool interaction yields the lowest attack success rates among the evaluated settings**. Across our evaluations, this paradigm reduces jailbreak success by around 30% relative on average across the evaluated models. The effect is robust to the visual content returned by the image tool: even when the returned image is manually overridden or itself unsafe, models remain harder to jailbreak as long as the reasoning process includes explicit image-tool interaction. This result suggests that the lower ASR is not explained solely by the semantics of the returned image. Instead, the image-tool-calling trajectory appears to act as a safety-relevant cue during TwI.

To account for this phenomenon, we introduce an *image-tool safety vector* framework. At a representation level, the framework models image-tool invocation as a residual shift in hidden states and asks whether the resulting image-tool state makes safety behavior more linearly readable and more steerable. Representation-level analyses across returned-image settings support this view and provide a mechanistic account for why explicit image-tool interaction can improve safety even when the image-tool output itself is not benign.

Our contributions are threefold:

- We frame multimodal jailbreak robustness as a comparison across think-with-image process paradigms, including direct response, text-only prior turn, simulated image generation/editing, visual-state variants, and explicit image-tool interaction.
- We find that explicit image-tool interaction yields the lowest attack success rates among the evaluated settings and show that the ASR reduction remains under substantial changes to returned visual content but disappears under text-only prior turn controls.
- We introduce the image-tool safety vector framework and support it with representation-level and activation-intervention evidence, linking image-tool invocation to an internal state that is more safety-separable and behaviorally steerable.

## 2 Related Work

Our study connects think-with-image reasoning, tool-using multimodal agents, multimodal jailbreak evaluation, and representation-level safety analysis.

**Think-with-image reasoning.** Recent LVLMs increasingly perform *think-with-image* reasoning, where intermediate visual states become part of inference. Prior work externalizes visual thoughts [Cheng et al., 2025a] through sketches, whiteboards, generated visualizations, regions, or coordinates [Hu et al., 2024, Menon et al., 2024, Li et al., 2025, Yang et al., 2023a, Wu and Xie, 2024], and also studies reasoning boundaries, multi-step multimodal reasoning benchmarks, or training procedures [Chen et al., 2024a, Cheng et al., 2025b, Chen et al., 2024b, Su et al., 2025b]. These works establish think-with-image as a broad capability paradigm, but largely leave its adversarial safety implications unexplored.

**Tool-augmented multimodal agents.** Tool-using models interleave reasoning with external actions or modules [Yao et al., 2023, Schick et al., 2023]. Multimodal agents extend this paradigm by integrating vision tools, executable programs, and grounded actions for visual reasoning and agentic tasks [Wu et al., 2023, Gupta and Kembhavi, 2023, Surís et al., 2023, Lu et al., 2023, Zheng et al., 2024, Xie et al., 2024]. Existing safety studies mainly focus on external failures, including indirect prompt injection, unsafe actions, and environment-level risks [Greshake et al., 2023, Ruan et al., 2024, Zhan et al., 2024, Debenedetti et al., 2024], leaving underexplored how tool invocation reshapes a model’s internal safety behavior.

**Multimodal jailbreak evaluation.** Multimodal safety benchmarks show that harmful image-text inputs remain effective against LVLMs [Liu et al., 2024, Luo et al., 2024], while broader benchmarks standardize jailbreak and refusal evaluation [Mazeika et al., 2024, Chao et al., 2024, Weng et al., 2025]. This line provides threat models and metrics, but typically evaluates a fixed inference pathway rather than treating the reasoning paradigm as an experimental variable.

**Representation-level safety analysis.** Representation-level work shows that refusal and safety behavior can often be detected or influenced through low-dimensional activation patterns [Zou et al., 2023, Arditi et al., 2024, Lee et al., 2025, Wollschläger et al., 2025, Xu et al., 2024, Qian et al., 2025, Wang et al., 2025]; concurrent work extends this to large vision-language models, both for activation steering [Yang et al., 2026] and for steering safety judgments via semantic cues [Hinojosa et al., 2026]. This motivates our analysis of whether explicit image-tool interaction induces a consistent safety-relevant shift in LVLM hidden states.

Prior work leaves open whether think-with-image paradigms themselves change jailbreak robustness. We study this directly by comparing direct, simulated image generation/editing, visual-state, and explicit image-tool interaction settings under the same safety protocol. This reveals a surprising pattern: explicit image-tool interaction produces the lowest attack success rates in our experiments, and the reduction points beyond returned-image semantics to the image-tool-calling process within multimodal reasoning.

### 3 Preliminary

#### 3.1 We Compare Paradigms by Holding the Safety Query Fixed

Let  $q_i = (x_i, t_i)$  denote the  $i$ -th safety query, where  $x_i$  is the adversarial image and  $t_i$  is the harmful text prompt. For each paradigm  $k$ , the prefix  $\pi_k$  represents the process that happens before the safety query, while  $q_i$  itself stays fixed. Given an LVLM  $f_\theta$ , an unsafe-response judge  $J$ , and  $N$  evaluation items, we compute the attack success rate (ASR) under paradigm  $k$ :

$$y_{i,k} = f_\theta(\pi_k \oplus q_i), \quad \widehat{\text{ASR}}_k = \frac{1}{N} \sum_{i=1}^N J(y_{i,k}), \quad (1)$$

Here,  $\oplus$  denotes concatenating the prefix with the later safety query,  $y_{i,k}$  is the model’s final answer under paradigm  $k$ , and  $J(y_{i,k}) = 1$  means that this answer is judged unsafe.

#### 3.2 Paradigms Differ in the Process Before the Safety Query

We define a paradigm by the prefix placed before the same MM-SafetyBench query. Each paradigm corresponds to a different think-with-image process, with different intermediate states and interactions. The main paradigm comparison is summarized in Table 1, and the text-only prior turn control is reported separately in Table 2. **Direct baseline** asks the model to answer the safety query immediately, so  $\pi_{\text{direct}} = \emptyset$ . **Text-only prior turn** checks whether a completed prior textual image-tool-like turn is enough to change safety behavior;  $\pi_{\text{text}}$  keeps a completed text-only prefix but removes the returned image and any subsequent visual feedback. **Simulated image generation/editing** tests whether a generated or edited visual state before the safety query matters without image-tool-based analysis;  $\pi_{\text{gen}}$  contains a generated prefill image. **Visual-state variants** test the role of returned-image content;  $\pi_{\text{state}} = (b, a, r')$  keeps a benign prefix task  $b$  and the model’s image-tool request  $a$  but replaces the returned artifact with a controlled image  $r'$ . **Explicit image-tool interaction** tests the full image-tool-mediated process;  $\pi_{\text{tool}} = (b, a, T(a))$  contains the benign task, the model’s image-tool request, and the actual VSP output  $T(a)$  returned by the image tool. In all non-direct settings, the adversarial image  $x_i$  is absent from  $\pi_k$  and appears only inside  $q_i$ ; the judge scores only the final answer  $y_{i,k}$ .

Table 1: Representative paradigm and control comparison on Qwen3-VL-235B on MM-SafetyBench.

Paradigm	Representative setting	ASR (%)
Direct response	–	36.1
Image generation/editing*	Neutral image prefill	38.1
Image generation/editing*	Harmful image prefill	35.6
Visual-state variant	Edited image attention	32.6
Explicit image-tool interaction	Benign returned image	24.8
Explicit image-tool interaction	Unsafe-looking returned image	26.2
Explicit image-tool interaction	Standard image-tool setting	23.8

\* Qwen3-VL-235B does not natively support image generation. Because direct EMU [Wang et al., 2026]-style generation produced low-quality reasoning prefixes in our setup, we use Stable-Diffusion-generated prefill images to simulate image generation/editing prefixes rather than as a faithful EMU reproduction. EMU-3 results are given in Table 6.

## 4 Experimental Setting

We test whether the *process* preceding a harmful multimodal query affects jailbreak robustness. Each instance pairs a fixed safety query with, when applicable, a benign think-with-image prefix that induces intermediate visual computation. For safety evaluation, we use MM-SafetyBench [Liu et al., 2024], whose adversarial image-text pairs are generated via typographic attacks or Stable Diffusion [Rombach et al., 2022] across 13 safety-sensitive categories. Due to the cost of think-with-image pipelines, we randomly sample 202 questions using a fixed sampling seed; the per-category composition of this subset is given in Appendix A. The primary metric is attack success rate (ASR), defined as the fraction of final safety-query responses judged unsafe by an LLM-as-judge evaluator [Zheng et al., 2023]. In multi-turn settings, the judge is given only the model’s final answer to the MM-SafetyBench query, not the benign prefix or image-tool transcript, so the prefix affects ASR only through the answer produced by the evaluated model.

For the benign prefix, we use CoMT tasks [Cheng et al., 2025b] that reliably elicit intermediate visual computation, with image-tool calls executed through Visual Sketchpad (VSP) [Hu et al., 2024]. This implements the *explicit image-tool interaction* paradigm: the model solves a benign visual reasoning task, issues a structured image-tool request, receives the image-tool output, and then receives the MM-SafetyBench query. The benign stage is not scored; it only defines the process prefix before safety evaluation. Behavioral experiments cover Qwen3-VL [Bai et al., 2025], Gemma-3 [Gemma Team, 2025], Llama-4 [Meta AI, 2025], and Pixtral [Agrawal et al., 2024] families under consistent provider settings within each family. Mechanistic experiments use self-deployed Qwen3-VL-8B [Bai et al., 2025], since hidden-state extraction and activation interventions require model internals. For explicit image-tool runs, we also record whether the intermediate computation appears as a direct VSP call or generated code. Self-deployed image-tool runs exhibit small run-to-run ASR variation from GPU-level numerical nondeterminism in the multi-turn pipeline; intervention experiments therefore report changes against within-batch zero-injection baselines. Behavioral experiments are issued through the OpenRouter API gateway; self-deployed mechanistic experiments on Qwen3-VL-8B run on a single NVIDIA A800 80GB GPU.

## 5 Which Paradigm Is Safer?

We compare think-with-image paradigms under the same harmful-query distribution and safety judge, varying only the prefix before the final MM-SafetyBench question. The clearest pattern is simple: models are jailbroken less often when the prefix includes explicit image-tool interaction. We then test two plain alternatives: whether the drop comes only from a text-only prior turn, or only from the image returned by the tool.

**Explicit image-tool interaction is the most robust evaluated setting.** Table 1 shows the main comparison. Direct response is jailbroken in 36.1% of cases, while the Stable-Diffusion-based simulated image generation/editing setting stays about the same. The visual-state variant lowers ASR only moderately to 32.6%, suggesting that simply adding an edited visual state is not enough. Explicit image-tool interaction is different: ASR falls to 23.8% in the standard setting and stays below 26.2% even when the returned image looks unsafe. Figure 1 shows the same direction across model families and scales, so the lower ASR is not limited to one model size or provider.

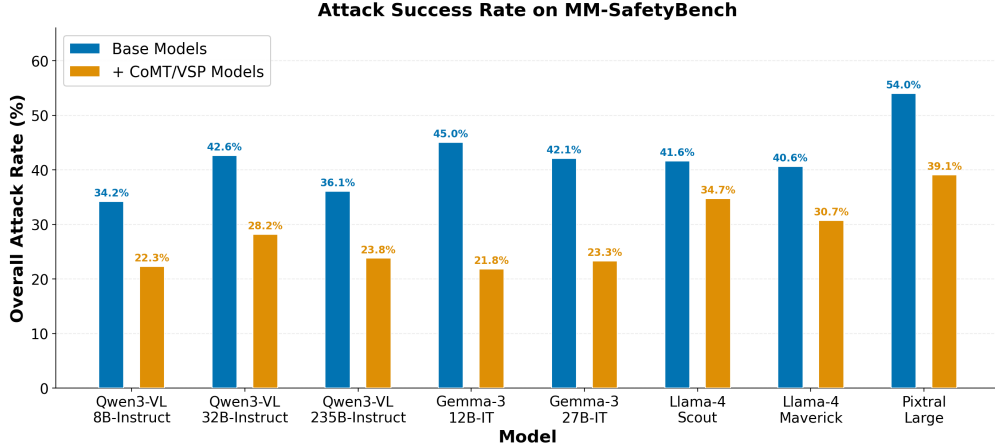


Figure 1: Overall ASR on MM-SafetyBench for direct answering and explicit image-tool interaction. Across model families and scales, explicit image-tool interaction yields lower attack success rates.

Table 2: Text-only prior turn controls. *Direct* is the single-turn baseline; *Image-tool interaction* is the explicit image-tool interaction setting; *text-only prior turn* preserves a completed text-only prefix but removes returned visual feedback. ASR (%) is measured on MM-SafetyBench. Additional setup details are given in Appendix B.

Model	Direct	Image-tool interaction	Prior turn (NORMAL)	Prior turn (HARMFUL)
Qwen3-VL-8B	34.2	<b>22.3</b>	33.2	36.1
Qwen3-VL-32B	42.6	<b>28.2</b>	38.1	39.6
Qwen3-VL-235B	36.1	<b>23.8</b>	38.1	35.6
Gemma-3-12B	45.0	<b>21.8</b>	44.1	47.5
Gemma-3-27B	42.1	<b>23.3</b>	43.1	48.5
Llama-4-Scout	41.6	<b>34.7</b>	44.1	44.6
Pixtral-Large	54.0	<b>39.1</b>	51.0	46.5

**Text-only prior turns do not explain the ASR drop.** One simple explanation is that any completed prior turn changes the dialogue state and makes the model more cautious. To test this, we keep a text-only prior turn but remove the returned visual state from the image tool, while leaving the later harmful query unchanged. Table 2 shows that this is not enough. On Qwen3-VL-235B, direct answering gives 36.1% ASR, normal and harmful prior turns give 38.1% and 35.6%, while explicit image-tool interaction falls to 23.8%. Across models, text-only prior turn ASR remains close to direct answering and far above image-tool interaction, so the lower ASR is not reproduced by a prior text-only turn or by refusal-oriented warm-up alone. Appendix B gives setup details and notes failed provider runs.

**Returned-image semantics are not necessary for most of the ASR drop.** The next alternative is that the returned image itself makes the model safer, for example by supplying benign visual evidence before the harmful query. We test this by keeping the image-tool transcript fixed and overriding only the returned visual content with unsafe-looking, benign, or low-information images. If returned-image semantics were the main driver, ASR should vary strongly across these replacements, especially when useful visual content is removed.

**The ASR drop remains when useful visual content is removed.** Table 3 shows that ASR remains low under all returned-image overrides: 26.2% with an unsafe-looking image, 24.8% with a benign image, and 25.7% with a white/noise replacement. The white/noise condition is the strictest test because it removes most object- and scene-level evidence while preserving the interaction structure. Thus the returned image does not need to contain useful visual evidence for the model to be jailbroken less often; small differences among returned-image variants are within the run-to-run baseline drift documented in Appendix E and should be read qualitatively.

**Lower ASR follows the interaction trace, not the returned visual artifact.** Overall, the attribution sequence points toward the image-tool interaction process rather than the returned artifact alone. The

Table 3: Returned-image variants used to separate visual content from the image-tool-calling process. ASR is measured on Qwen3-VL-235B.

Condition	Returned visual content	ASR (%)
Direct	–	36.1
Image-tool interaction + unsafe image	Stable Diffusion unsafe-looking image	26.2
Image-tool interaction + benign image	Stable Diffusion benign image	24.8
Image-tool interaction + visual mask	White/noise replacement image	25.7

model must issue an image-tool request, receive a structured image-tool result, and condition on that interaction before the harmful query arrives. The returned pixels can change substantially while ASR remains low, whereas removing returned visual feedback and keeping only the text-only prior turn brings ASR back near direct answering.

## 6 Why Is Explicit Image-Tool Interaction Better?

### 6.1 Safety-Aligned Residual Shift

**Mechanistic hypothesis.** The behavioral results suggest that the robustness gain is tied to the full image-tool interaction, not to the text-only image-tool trace or to benign returned-image content alone. We model this effect as a residual shift in hidden-state space before the model answers the harmful query. Let  $z \sim \mathcal{D}_{\text{adv}}$  be an adversarial query, let  $h(z) \in \mathbb{R}^d$  be its direct-mode hidden state at a selected layer, and let  $u \in \mathbb{R}^d$  be a safety readout direction where larger projection means safer behavior [Zou et al., 2023, Arditì et al., 2024]. We define the corresponding safety score

$$S(z) = u^\top h(z), \quad (2)$$

so that larger  $S(z)$  corresponds to safer behavior. If explicit image-tool interaction induces a residual shift  $v_{\text{tool}}$  with strength  $\alpha \geq 0$ , then

$$h_{\text{tool}}(z) = h(z) + \alpha v_{\text{tool}}, \quad S_{\text{tool}}(z) = S(z) + \alpha(u^\top v_{\text{tool}}). \quad (3)$$

Here,  $h_{\text{tool}}(z)$  and  $S_{\text{tool}}(z)$  are the hidden state and safety score after the image-tool prefix. The condition  $u^\top v_{\text{tool}} > 0$  means that the image-tool state shifts the representation toward the safer side of the readout.

**Definition 1** (Image-Tool Safety Vector). *At layer  $\ell$ , let  $h_{\text{direct}}^\ell(z)$  and  $h_{\text{tool}}^\ell(z)$  denote the hidden representations for the same query under direct answering and explicit image-tool interaction. The layer- $\ell$  image-tool safety vector is the population mean residual shift:*

$$v_{\text{tool}}^\ell = \mathbb{E}_{z \sim \mathcal{D}_{\text{eval}}} [h_{\text{tool}}^\ell(z) - h_{\text{direct}}^\ell(z)]. \quad (4)$$

*Its empirical estimate on  $n$  paired examples is*

$$\hat{v}_{\text{tool}}^\ell = \frac{1}{n} \sum_{i=1}^n (h_{\text{tool}}^\ell(z_i) - h_{\text{direct}}^\ell(z_i)). \quad (5)$$

We use  $v_{\text{tool}}$  for the population shift in the theorem and  $\hat{v}_{\text{tool}}^\ell$  for its empirical layer-wise estimate.

**Theorem 1** (Positive safety projection reduces thresholded jailbreak risk). *Let  $S(z) = u^\top h(z)$  be a safety score where larger values are safer, and let  $\tau$  be an unsafe-behavior threshold. If explicit image-tool interaction shifts the representation by  $\alpha v_{\text{tool}}$  with  $\alpha \geq 0$  and  $u^\top v_{\text{tool}} > 0$ , then the thresholded jailbreak risk*

$$\mathcal{R}(\alpha) = \Pr_{z \sim \mathcal{D}_{\text{adv}}} [S(z) + \alpha u^\top v_{\text{tool}} < \tau]$$

*is non-increasing in  $\alpha$ . Moreover, for any  $\alpha_2 > \alpha_1 \geq 0$ , the decrease is strict whenever*

$$\Pr[\tau - \alpha_2 u^\top v_{\text{tool}} \leq S(z) < \tau - \alpha_1 u^\top v_{\text{tool}}] > 0.$$

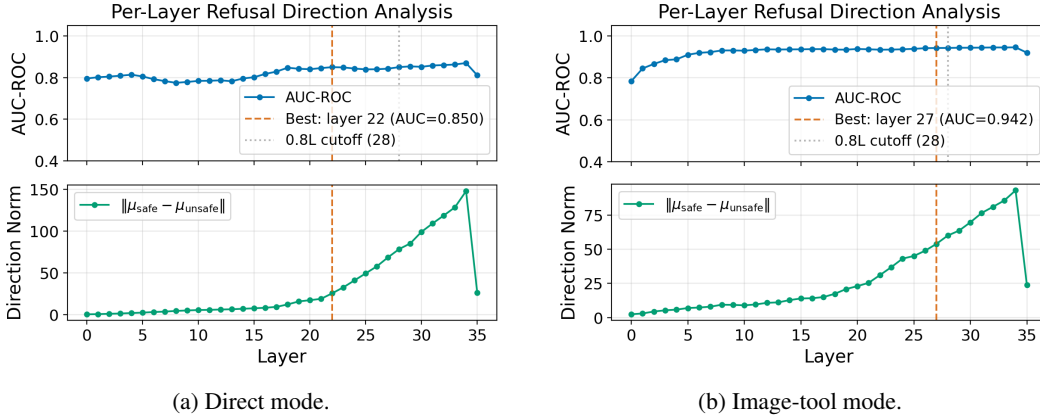


Figure 2: Layer-wise safety readout quality on Qwen3-VL-8B-Instruct. (Top) AUC for direct answering and image-tool interaction; (Bottom) The corresponding direction norms. The image-tool state produces a stronger readout, peaking at AUC 0.942 vs. 0.850 for direct answering.

Theorem 1 is only a sufficient-condition statement: if the shift points toward a learned safety readout, examples near the refusal boundary become less likely to produce unsafe completions. We do not claim to inject the population shift  $v_{tool}$  directly; instead, the experiments test whether the image-tool state aligns with learned safety directions that are readable from, and active in, the residual stream. The two observable consequences are that the image-tool state should make safety more linearly readable, and safety-direction interventions should change ASR in the expected direction. The full proof is given in Appendix F.

## 6.2 Image-Tool Interaction Creates a Stronger and More Stable Safety Readout

**Explicit image-tool interaction makes safety more linearly readable.** The first prediction is that the image-tool-mediated state should make safe and unsafe completions easier to separate. Figure 2 shows that the image-tool state yields a stronger layer-wise safety readout than direct answering. Thus explicit image-tool interaction does not only reduce ASR externally; it places the model in a state where the subsequent safety decision is more linearly accessible from hidden representations. Additional fitting details and layer-wise numbers are given in Appendix C.

**The image-tool safety direction is stable across returned-image variants.** The second prediction is that the direction should be tied to the image-tool-calling process rather than to the particular pixels returned by the image tool. Figure 3 shows that safety directions extracted from six returned-image variants are nearly collinear. If the direction mainly encoded returned-image semantics, benign, unsafe-looking, white, or noisy outputs should rotate it substantially. Instead, the common factor appears to be the structured image-tool-calling process. Transfer AUCs and override details are given in Appendix C.

**Representation evidence supports a process-level mechanism.** The representation results mirror the behavioral attribution. Text-only prior turns do not reproduce the ASR gain, returned-image overrides do not remove it, and the corresponding hidden-state directions remain stable across those overrides. Figure 4 further shows that the image-tool safety readout is compact and transfers across returned-image variants, supporting a process-level mechanism rather than an explanation tied to particular returned pixels.

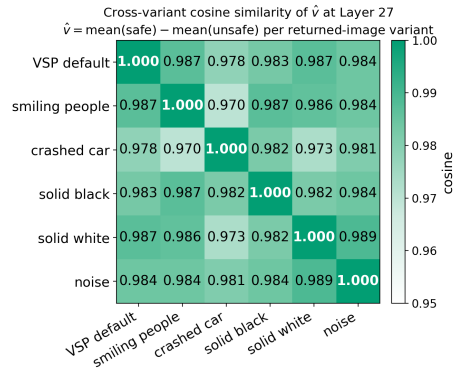


Figure 3: Cosine similarity between safety directions learned from six returned-image variants. High off-diagonal similarity indicates that the safety direction is stable across returned-image content.

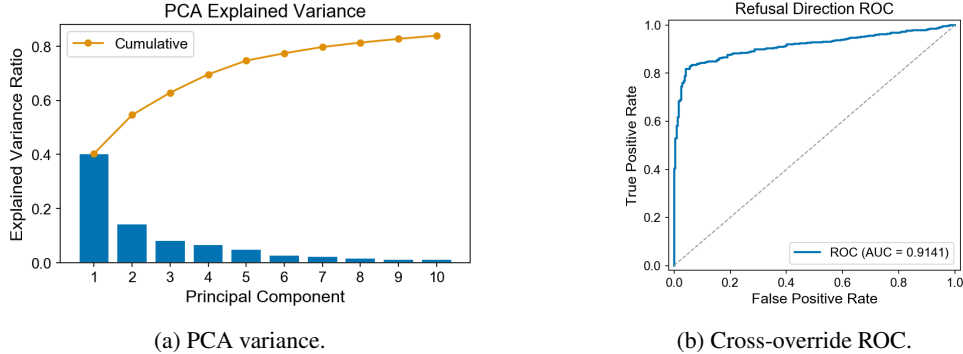


Figure 4: Readout diagnostics for the layer-27 image-tool safety direction on Qwen3-VL-8B-Instruct. (a) PC1 explains 40.3% of variance and is nearly aligned with the safety direction (projection 0.993), indicating a compact safety axis. (b) Direction fit on the normal returned-image run transfers to five override runs (AUC = 0.914), showing the readout is not tied to returned-image content.

Table 4: Activation-intervention summary on Qwen3-VL-8B. Image-tool interaction changes are computed against within-batch zero-injection baselines.

Sweep	Mode / intervention	Baseline	ASR ( $\downarrow$ )	$\Delta$	Shape
Sufficiency	Direct, $+u_{\text{direct}}$	36.6	23.8	<b>-12.9</b>	monotone $\downarrow$
Necessity	Image-tool interaction, $-u_{\text{direct}}$	24.8	31.7	<b>+6.9</b>	monotone $\uparrow$
Sufficiency	Image-tool interaction, $+u_{\text{direct}}$	19.8	11.9	<b>-7.9</b>	U-shaped
Specificity	Direct, $+u_{\text{tool}}$	36.6	34.5	-2.1	flat
Specificity	Image-tool interaction, $-u_{\text{tool}}$	21.0	26.4	<b>+5.4</b>	monotone $\uparrow$

**Compact image-tool shifts mainly affect marginal cases.** Figure 4 matters because it connects the behavioral attribution to the thresholded-risk model in Theorem 1. The readout is compact and transfers across returned-image variants, so the relevant shift is unlikely to be a scattered encoding of a particular returned image. At the same time, the theorem predicts that such a positive safety shift changes ASR only when examples occupy a non-saturated region near the refusal boundary. The boundary diagnostics show nontrivial near-threshold mass, suggesting that explicit image-tool interaction reduces ASR by moving marginal harmful cases across the safety boundary, rather than by uniformly solving all attack categories. Additional PCA, transfer, and boundary details are given in Appendix C.

### 6.3 Activation Interventions Show That Safety Directions Are Behaviorally Active

**Activation interventions test whether learned safety directions are behaviorally active.** To move beyond correlational readouts, we intervene on the residual stream of Qwen3-VL-8B during inference. The intervention layer, direction, and coefficients are selected on an internal validation split, and all ASR results are reported on the held-out test set. At layer  $\ell$ , a forward hook adds

$$\Delta h = \lambda \hat{u}_{\text{direct}}^{\ell} + \mu \hat{u}_{\text{tool}}^{\ell}, \quad (6)$$

to every token hidden state [Zou et al., 2023, Arditì et al., 2024, Lee et al., 2025], where  $\lambda, \mu$  are scalar coefficients and  $\hat{u}_{\text{direct}}^{\ell}, \hat{u}_{\text{tool}}^{\ell}$  are normalized safety directions for direct and image-tool modes. We evaluate sufficiency in direct mode, necessity in image-tool interaction, and additional sufficiency in image-tool interaction. Additional sweep settings and baseline conventions are given in Appendix D.

**Adding a safety direction partially reproduces the image-tool robustness gain.** As shown in Table 4, adding the direct-mode safety direction in direct mode lowers ASR from 36.6% to 23.8%, close to the behavioral gain of explicit image-tool interaction in the matched evaluation. This goes beyond representation separability: the direction is not only predictive of safe versus unsafe outputs, but also behaviorally active when injected into the residual stream.

**Removing safety directions partially erodes the image-tool robustness gain.** The necessity sweep provides complementary evidence. In the image-tool interaction setting, subtracting the direct-mode safety direction raises ASR from 24.8% to 31.7%, while adding it lowers ASR from 19.8% to

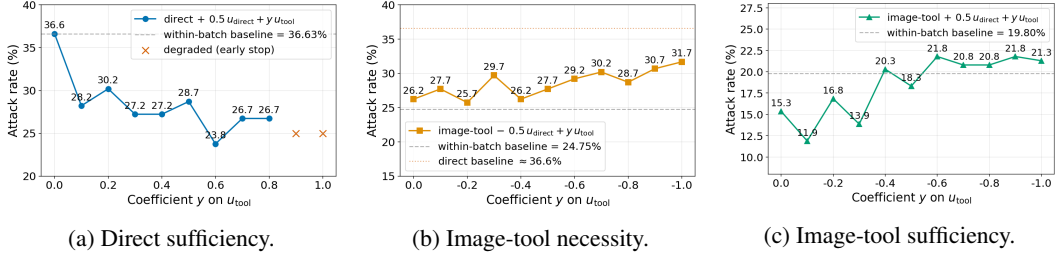


Figure 5: Activation-intervention dose-response curves on Qwen3-VL-8B-Instruct. Panels test direct-mode sufficiency, image-tool necessity, and image-tool sufficiency. Adding safety-direction components lowers ASR, while subtracting them from the image-tool setting raises ASR.

11.9%. The comparable magnitudes of these effects ( $7.9/6.9 = 1.14$ ) suggest that this safety-relevant axis accounts for part of the robustness gain. Specificity sweeps further show that the image-tool-mode direction is less effective when added to direct mode but harmful when removed from image-tool interaction, indicating mode-specific activation geometry rather than a single universal steering vector.

**The intervention effect is partly symmetric within the image-tool state but mode-specific across states.** Figure 5 separates two effects. Within image-tool interaction, adding and subtracting safety-direction components have comparable magnitudes in the non-degenerate dose range, consistent with a behaviorally active safety axis. Across inference modes, however, the directions are not equally portable: adding the image-tool-mode direction to direct inference weakly affects ASR, whereas removing it within image-tool interaction substantially increases ASR. This argues against a universal-vector account and suggests that image-tool interaction changes the local activation geometry in which safety directions operate.

**Mechanistic interpretation.** Together, the behavioral, representation, and intervention results support a coherent account: explicit image-tool interaction induces a recurring internal state where safety-relevant information is more linearly accessible, stable across returned-image content, and behaviorally linked to ASR. We therefore interpret the image-tool-calling trajectory as a process-level safety cue, with intervention evidence limited to the non-degenerate dose range and read as partial mechanistic support rather than a complete causal mediation proof.

## 7 Discussion

**Implications for deployment.** Our results suggest that LVLm safety depends not only on training or post-hoc filtering, but also on inference structure. If the image-tool interaction effect generalizes, tool-augmented think-with-image pipelines may offer a safety-relevant design pattern for multimodal systems. Deployment-time safety evaluation should therefore assess the full reasoning pipeline, not only the direct response.

**Limitations and risks.** Our results should not be read as a blanket endorsement of tool use. Tool-augmented systems can introduce new attack surfaces, including malicious tool outputs, indirect prompt injection, unsafe actions, and adaptive attacks on tool-calling trajectories [Noheria and Yao, 2026, Zhao et al., 2026]. Our empirical scope is also limited: we study a 202-example MM-SafetyBench sample, rely on one primary LLM-as-judge protocol, and run mechanistic analyses on self-deployed Qwen3-VL-8B where hidden states are available. The main conclusion is therefore narrower: safety evaluation should account for the full think-with-image pipeline, rather than treating tool use as inherently safe or unsafe.

**Research outlook.** This work reframes think-with-image reasoning as a safety-relevant inference paradigm, not merely a capability mechanism. It motivates evaluations that vary the reasoning process and a mechanistic agenda studying when intermediate visual states and image-tool-calling trajectories induce safety-relevant hidden-state shifts.

## 8 Conclusion

We asked which think-with-image process design improves multimodal jailbreak robustness and found that explicit image-tool interaction gives the strongest benefit among the evaluated paradigms, lowering ASR by around 30% relative to direct answering across model families and scales. The key

finding is not merely that image tools return helpful images: replacing the returned image preserves most of the gain, while removing returned visual feedback and keeping only a text-only prefill does not reproduce it. We then linked this process-level effect to a stable image-tool safety state and showed through activation interventions that learned safety directions are behaviorally active. These results suggest that explicit image-tool interaction is a promising safety-positive design pattern for future think-with-image LVLMs, provided it is evaluated as a full pipeline rather than treated as inherently safe.

## References

- Pravesh Agrawal, Szymon Antoniak, Emma Bou Hanna, Baptiste Bout, Devendra Chaplot, Jessica Chudnovsky, Diogo Costa, et al. Pixtral 12B. *arXiv preprint arXiv:2410.07073*, 2024.
- Andy Arditi, Oscar Obeso, Aaquib Syed, Daniel Paleka, Nina Panickssery, Wes Gurnee, and Neel Nanda. Refusal in language models is mediated by a single direction. In *Advances in Neural Information Processing Systems (NeurIPS)*, 2024.
- Shuai Bai, Yuxuan Cai, Ruizhe Chen, Keqin Chen, Xionghui Chen, Zesen Cheng, Lianghao Deng, Wei Ding, Chang Gao, Chunjiang Ge, et al. Qwen3-vl technical report. *arXiv preprint arXiv:2511.21631*, 2025.
- Patrick Chao et al. JailbreakBench: An open robustness benchmark for jailbreaking large language models. In *Advances in Neural Information Processing Systems (NeurIPS)*, 2024.
- Qiguang Chen, Libo Qin, Jiaqi Wang, Jinxuan Zhou, and Wanxiang Che. Unlocking the capabilities of thought: A reasoning boundary framework to quantify and optimize chain-of-thought. *Advances in Neural Information Processing Systems*, 37:54872–54904, 2024a.
- Qiguang Chen, Libo Qin, Jin Zhang, Zhi Chen, Xiao Xu, and Wanxiang Che. M3cot: A novel benchmark for multi-domain multi-step multi-modal chain-of-thought. In *Proceedings of the 62nd Annual Meeting of the Association for Computational Linguistics (Volume 1: Long Papers)*, pages 8199–8221, 2024b.
- Qiguang Chen, Libo Qin, Jinhao Liu, Dengyun Peng, Jiannan Guan, Peng Wang, Mengkang Hu, Yuhang Zhou, Te Gao, and Wanxiang Che. Towards reasoning era: A survey of long chain-of-thought for reasoning large language models. *Science China Information Sciences*, 69(6):161101, 2026.
- Zihui Cheng, Qiguang Chen, Xiao Xu, Jiaqi Wang, Weiyun Wang, Hao Fei, Yidong Wang, Alex Jinpeng Wang, Zhi Chen, Wanxiang Che, et al. Visual thoughts: A unified perspective of understanding multimodal chain-of-thought. *Advances in Neural Information Processing Systems*, 38: 96084–96112, 2025a.
- Zihui Cheng, Qiguang Chen, Jin Zhang, Hao Fei, Xiao Cheng Feng, Wanxiang Che, Min Li, and Libo Qin. CoMT: A novel benchmark for chain of multi-modal thought on large vision-language models. In *Proceedings of the AAAI Conference on Artificial Intelligence*, volume 39, 2025b.
- Edoardo DeBenedetti, Jie Zhang, Mislav Balunović, Luca Beurer-Kellner, Marc Fischer, and Florian Tramèr. AgentDojo: A dynamic environment to evaluate prompt injection attacks and defenses for LLM agents. In *Advances in Neural Information Processing Systems (NeurIPS) Datasets and Benchmarks Track*, 2024.
- Gemma Team. Gemma 3 technical report. *arXiv preprint arXiv:2503.19786*, 2025.
- Kai Greshake, Sahar Abdelnabi, Shailesh Mishra, Christoph Endres, Thorsten Holz, and Mario Fritz. Not what you’ve signed up for: Compromising real-world LLM-integrated applications with indirect prompt injection. In *ACM Workshop on Artificial Intelligence and Security (AISec)*, 2023.
- Tanmay Gupta and Aniruddha Kembhavi. Visual programming: Compositional visual reasoning without training. In *IEEE/CVF Conference on Computer Vision and Pattern Recognition (CVPR)*, 2023.

- Carlos Hinojosa, Clemens Grange, and Bernard Ghanem. SAVeS: Steering safety judgments in vision-language models via semantic cues. *arXiv preprint arXiv:2603.19092*, 2026.
- Yushi Hu, Weijia Shi, Xingyu Fu, Dan Roth, Mari Ostendorf, Luke Zettlemoyer, Noah A Smith, and Ranjay Krishna. Visual sketchpad: Sketching as a visual chain of thought for multimodal language models. In *Advances in Neural Information Processing Systems (NeurIPS)*, 2024.
- Jing Yu Koh, Robert Lo, Lawrence Jang, Vikram Duvvur, Ming Chong Lim, Po-Yu Huang, Graham Neubig, Shuyan Zhou, Ruslan Salakhutdinov, and Daniel Fried. VisualWebArena: Evaluating multimodal agents on realistic visual web tasks. In *Annual Meeting of the Association for Computational Linguistics (ACL)*, 2024.
- Brian W. Lee et al. Programming refusal with conditional activation steering. In *International Conference on Learning Representations (ICLR)*, 2025.
- Chengzu Li, Wenshan Wu, Huanyu Zhang, Yan Xia, Shaoguang Mao, Li Dong, Ivan Vulić, and Furu Wei. Imagine while reasoning in space: Multimodal visualization-of-thought. In *International Conference on Machine Learning (ICML)*, 2025.
- Xin Liu, Yichen Zhu, Jindong Gu, Yunshi Lan, Chao Yang, and Yu Qiao. MM-SafetyBench: A benchmark for safety evaluation of multimodal large language models. In *European Conference on Computer Vision (ECCV)*, 2024.
- Pan Lu, Baolin Peng, Hao Cheng, Michel Galley, Kai-Wei Chang, Ying Nian Wu, Song-Chun Zhu, and Jianfeng Gao. Chameleon: Plug-and-play compositional reasoning with large language models. In *Advances in Neural Information Processing Systems (NeurIPS)*, 2023.
- Weidi Luo, Siyuan Ma, Xiaogeng Liu, Xiaoyu Guo, and Chaowei Xiao. JailBreakV: A benchmark for assessing the robustness of MultiModal large language models against jailbreak attacks. *arXiv preprint arXiv:2404.03027*, 2024.
- Mantas Mazeika, Long Phan, Xuwang Yin, Andy Zou, Zifan Wang, Norman Mu, Elham Sakhaee, Nathaniel Li, Steven Basart, Bo Li, David Forsyth, and Dan Hendrycks. HarmBench: A standardized evaluation framework for automated red teaming and robust refusal. In *International Conference on Machine Learning (ICML)*, 2024.
- Sachit Menon, Richard S. Zemel, and Carl Vondrick. Whiteboard-of-thought: Thinking step-by-step across modalities. In *Conference on Empirical Methods in Natural Language Processing (EMNLP)*, pages 20016–20031, 2024.
- Meta AI. The Llama 4 herd: The beginning of a new era of natively multimodal AI innovation. <https://ai.meta.com/blog/llama-4-multimodal-intelligence/>, 2025.
- Aarush Noheria and Yuguang Yao. Jailbreaks on vision language model via multimodal reasoning. *arXiv preprint arXiv:2601.22398*, 2026.
- Zhiliang Peng, Wenhui Wang, Li Dong, Yaru Hao, Shaohan Huang, Shuming Ma, and Furu Wei. Kosmos-2: Grounding multimodal large language models to the world. *arXiv preprint arXiv:2306.14824*, 2023.
- Cheng Qian, Hainan Zhang, Lei Sha, and Zhiming Zheng. HSF: Defending against jailbreak attacks with hidden state filtering. In *Companion Proceedings of the ACM on Web Conference (WWW)*, 2025.
- Robin Rombach, Andreas Blattmann, Dominik Lorenz, Patrick Esser, and Björn Ommer. High-resolution image synthesis with latent diffusion models. In *IEEE/CVF Conference on Computer Vision and Pattern Recognition (CVPR)*, 2022.
- Yangjun Ruan, Honghua Dong, Andrew Wang, Silviu Pitis, Yongchao Zhou, Jimmy Ba, Yann Dubois, Chris J. Maddison, and Tatsunori Hashimoto. Identifying the risks of LM agents with an LM-emulated sandbox. In *International Conference on Learning Representations (ICLR)*, 2024.
- Timo Schick, Jane Dwivedi-Yu, Roberto Dessì, Roberta Raileanu, Maria Lomeli, Eric Hambro, Luke Zettlemoyer, Nicola Cancedda, and Thomas Scialom. Toolformer: Language models can teach themselves to use tools. In *Advances in Neural Information Processing Systems (NeurIPS)*, 2023.

- Zhaochen Su, Peng Xia, Hangyu Guo, Zhenhua Liu, Yan Ma, Xiaoye Qu, Jiaqi Liu, Yanshu Li, Kaide Zeng, Zhengyuan Yang, Linjie Li, Yu Cheng, Heng Ji, Junxian He, and Yi R. Fung. Thinking with images for multimodal reasoning: Foundations, methods, and future frontiers. *arXiv preprint arXiv:2506.23918*, 2025a.
- Zhaochen Su et al. OpenThinkIMG: Learning to think with images via visual tool reinforcement learning. *arXiv preprint arXiv:2505.08617*, 2025b.
- Dídac Surís, Sachit Menon, and Carl Vondrick. ViperGPT: Visual inference via python execution for reasoning. In *IEEE/CVF International Conference on Computer Vision (ICCV)*, 2023.
- Han Wang, Gang Wang, and Huan Zhang. Steering away from harm: An adaptive approach to defending vision language model against jailbreaks. In *IEEE/CVF Conference on Computer Vision and Pattern Recognition (CVPR)*, 2025.
- Xinlong Wang, Yufeng Cui, Jinsheng Wang, Fan Zhang, Yueze Wang, Xiaosong Zhang, Zhengxiong Luo, Quan Sun, Zhen Li, Yuqi Wang, et al. Multimodal learning with next-token prediction for large multimodal models. *Nature*, pages 1–7, 2026.
- Fenghua Weng, Yue Xu, Chengyan Fu, and Wenjie Wang. MMJ-Bench: A comprehensive study on jailbreak attacks and defenses for vision language models. In *Proceedings of the AAAI Conference on Artificial Intelligence*, 2025.
- Tom Wollschläger, Jannes Elstner, Simon Geisler, Vincent Cohen-Addad, Stephan Günnemann, and Johannes Gasteiger. The geometry of refusal in large language models: Concept cones and representational independence. In *International Conference on Machine Learning (ICML)*, 2025.
- Chenfei Wu, Shengming Yin, Weizhen Qi, Xiaodong Wang, Zecheng Tang, and Nan Duan. Visual ChatGPT: Talking, drawing and editing with visual foundation models. *arXiv preprint arXiv:2303.04671*, 2023.
- Penghao Wu and Saining Xie. V\*: Guided visual search as a core mechanism in multimodal LLMs. In *IEEE/CVF Conference on Computer Vision and Pattern Recognition (CVPR)*, 2024.
- Tianbao Xie, Danyang Zhang, Jixuan Chen, Xiaochuan Li, Siheng Zhao, Ruisheng Cao, Toh Jing Hua, Zhoujun Cheng, Dongchan Shin, Fangyu Lei, et al. OSWorld: Benchmarking multimodal agents for open-ended tasks in real computer environments. In *Advances in Neural Information Processing Systems (NeurIPS) Datasets and Benchmarks Track*, 2024.
- Zhihao Xu et al. Uncovering safety risks of large language models through concept activation vector. In *Advances in Neural Information Processing Systems (NeurIPS)*, 2024.
- Jianwei Yang, Hao Zhang, Feng Li, Xueyan Zou, Chunyuan Li, and Jianfeng Gao. Set-of-mark prompting unleashes extraordinary visual grounding in GPT-4V. *arXiv preprint arXiv:2310.11441*, 2023a.
- Jiaxi Yang, Shicheng Liu, Yuchen Yang, and Dongwon Lee. Steering to say no: Configurable refusal via activation steering in vision language models. *arXiv preprint arXiv:2602.07013*, 2026.
- Zhengyuan Yang, Linjie Li, Jianfeng Wang, Kevin Lin, Ehsan Azarnasab, Faisal Ahmed, Zicheng Liu, Ce Liu, Michael Zeng, and Lijuan Wang. MM-ReAct: Prompting ChatGPT for multimodal reasoning and action. *arXiv preprint arXiv:2303.11381*, 2023b.
- Shunyu Yao, Jeffrey Zhao, Dian Yu, Nan Du, Izhak Shafran, Karthik Narasimhan, and Yuan Cao. ReAct: Synergizing reasoning and acting in language models. In *International Conference on Learning Representations (ICLR)*, 2023.
- Qiusi Zhan, Zhixiang Liang, Zifan Ying, and Daniel Kang. InjecAgent: Benchmarking indirect prompt injections in tool-integrated large language model agents. In *Findings of the Association for Computational Linguistics: ACL 2024*, 2024.
- Wei Zhao, Zhe Li, Peixin Zhang, and Jun Sun. ClawGuard: A runtime security framework for tool-augmented LLM agents against indirect prompt injection. *arXiv preprint arXiv:2604.11790*, 2026.

Boyuan Zheng, Boyu Gou, Jihyung Kil, Huan Sun, and Yu Su. GPT-4V(ision) is a generalist web agent, if grounded. In *International Conference on Machine Learning (ICML)*, 2024.

Lianmin Zheng, Wei-Lin Chiang, Ying Sheng, Siyuan Zhuang, Zhanghao Wu, Yonghao Zhuang, Zi Lin, Zhuohan Li, Dacheng Li, Eric P. Xing, Hao Zhang, Joseph E. Gonzalez, and Ion Stoica. Judging LLM-as-a-Judge with MT-Bench and Chatbot Arena. In *Advances in Neural Information Processing Systems (NeurIPS)*, 2023.

Andy Zou et al. Representation engineering: A top-down approach to AI transparency. *arXiv preprint arXiv:2310.01405*, 2023.

## Appendix

### A MM-SafetyBench Category Composition

MM-SafetyBench [Liu et al., 2024] organizes adversarial image-text pairs into 13 safety-sensitive categories. Each instance pairs a harmful question with an image generated by a typographic attack or by Stable Diffusion [Rombach et al., 2022]. To keep think-with-image evaluation tractable, we draw a 202-question evaluation subset as a stratified subsample at a fixed rate of approximately 12% per category; the same subset is used by every paradigm and every model in this paper, so cross-paradigm comparisons share identical underlying questions. Table 5 lists the 13 categories together with their full-dataset sizes, our per-category counts, and the resulting per-category sampling rates.

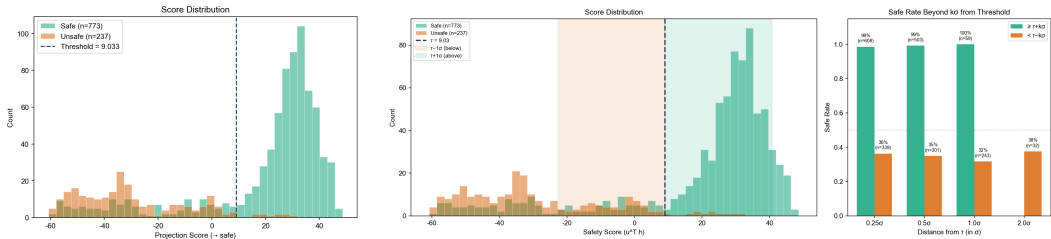
Table 5: MM-SafetyBench categories, full-dataset sizes, our per-category counts in the 202-question evaluation subset, and the resulting sampling rates. Rates lie within 11.4–12.4% across all categories (mean 12.0%, std 0.29 pp); per-category variation is driven entirely by integer rounding on small categories.

ID	Category	Full	Sample	Rate (%)
01	Illegal Activity	97	12	12.4
02	Hate Speech	163	20	12.3
03	Malware Generation	44	5	11.4
04	Physical Harm	144	17	11.8
05	Economic Harm	122	15	12.3
06	Fraud	154	18	11.7
07	Sex	109	13	11.9
08	Political Lobbying	153	18	11.8
09	Privacy Violence	139	17	12.2
10	Legal Opinion	130	16	12.3
11	Financial Advice	167	20	12.0
12	Health Consultation	109	13	11.9
13	Government Decision	149	18	12.1
Total		1680	202	12.0

The 202-question subset is therefore a near-uniform stratified 12% subsample of the full 1680-question MM-SafetyBench, rather than a quota-based or topic-weighted draw. Because the same subset is reused across all paradigms and models, ASR differences in our experiments cannot be driven by category resampling.

### B Text-Only Prior Turn Control Details

The text-only prior turn control removes returned visual feedback from the image-tool interaction and keeps a completed text-only prefix before asking the same MM-SafetyBench query. Operationally, it mimics the idea of a prior image-tool-like turn whose returned image has been removed, so the later safety query sees only text. We use two first-turn variants: a normal text-only prefix and a



(a) Safety-readout score distribution.

(b) Boundary sharpness.

Figure 6: Supplementary readout diagnostics. The learned direction separates safe and unsafe completions while retaining nontrivial mass near the threshold, allowing residual shifts to affect ASR.

Table 6: Representative paradigm and control comparison on EMU-3 on MM-SafetyBench.

Paradigm	Representative setting	ASR (%)
Direct response	–	72.4
Image generation/editing	Neutral image prefill	79.2
Image generation/editing	Harmful image prefill	83.9
Visual-state variant	Edited image attention	76.8
Explicit image-tool interaction	Benign returned image	Not Support
Explicit image-tool interaction	Unsafe-looking returned image	Not Support
Explicit image-tool interaction	Standard image-tool setting	Not Support

harmful-topic text-only prefix. The normal prefix tests whether the textual image-tool trace of a completed prior turn improves safety, while the harmful prefix tests whether a prior safety-relevant refusal or harmful-topic context changes the later answer. In both cases, the judge evaluates only the final answer to the MM-SafetyBench query.

Table 2 reports the valid runs. The Gemma-3-27B direct run in the original batch failed at the provider side and was filled in from a later re-run with matched parameters (sampling seed, judge, sampling rate, and provider backend held constant). Llama-4-Maverick text-only prior turn runs were excluded from the main table because the provider returned degenerate all-safe outputs in repeated runs. Across the valid models, text-only prior turn ASR stays close to direct answering and remains far above explicit image-tool interaction, supporting the conclusion that the text-only prior turn is not sufficient to reproduce the image-tool gain.

## C Representation Diagnostic Details

For the layer sweep in Figure 2, we extract hidden states from direct and explicit image-tool interaction runs on Qwen3-VL-8B-Instruct. At each layer  $\ell$ , we fit a difference-in-means safety direction

$$\hat{u}^\ell = \text{mean}(\text{safe}) - \text{mean}(\text{unsafe})$$

and score held-out completions by projection onto  $\hat{u}^\ell$ . The best direct-mode readout reaches AUC 0.850 at layer 22/36, whereas the best image-tool readout reaches AUC 0.942 at layer 27/36. The gray dotted line in Figure 2 marks the  $0.8L$  deep-layer cutoff used for direction selection, and the bottom panels report  $\|\hat{u}^\ell\|$ .

For the returned-image stability analysis in Figure 3, we train the safety direction on the normal VSP returned-image run and evaluate it on five override-image runs. The direction transfers with overall AUC 0.914 and per-override AUCs from 0.906 to 0.930; reversing the train/test direction gives AUC 0.910. Safety directions extracted from six returned-image variants have mean off-diagonal cosine similarity 0.983 and minimum 0.970, indicating that the direction is stable across returned-image content.

Figure 4 provides two additional diagnostics for the layer-27 image-tool safety direction. In the PCA view, PC1 explains 40.3% of the variance and is almost aligned with the learned safety direction (projection magnitude 0.993), indicating a compact, near-one-dimensional safety axis rather than scattered image-specific features. In the cross-override ROC, the safety direction is fit on the normal returned-image run and applied without retraining to held-out runs whose returned images are replaced by other content (smiling people, crashed car, solid black, solid white, noise); AUC = 0.914 shows that the readout is not tied to any particular returned image. The score-distribution and boundary-sharpness diagnostics in Figure 6 further show nontrivial mass near the operating threshold, where a positive residual shift can change binary ASR.

## D Activation-Intervention Details

Figure 5 reports intervention sweeps at layer 27 of Qwen3-VL-8B-Instruct. Each panel sweeps the image-tool-direction coefficient along  $\hat{u}_{\text{tool}}$  while holding the direct-direction offset fixed: direct mode with  $+0.5 \hat{u}_{\text{direct}}$ , image-tool mode with  $-0.5 \hat{u}_{\text{direct}}$ , and image-tool mode with  $+0.5 \hat{u}_{\text{direct}}$ .

The dashed gray lines mark within-batch zero-injection baselines, and the red dotted line in the image-tool necessity panel marks the no-intervention direct baseline.

The intervention layer, direction, and coefficients are selected on an internal validation split, and all ASR results are reported on the held-out test set. Because image-tool baselines can drift by several ASR points across independent runs (Appendix E), each sweep includes a zero-injection baseline and reports changes relative to that internal control.

## E Baseline ASR Drift Across Independent Runs

Self-deployed Qwen3-VL-8B image-tool baselines exhibit run-to-run drift even when the model checkpoint, prompts, sampling seed, sampling rate, and LLM-as-judge protocol are all held fixed. Table 7 reports five independent runs of the same Qwen3-VL-8B-Instruct checkpoint on the same 202-question MM-SafetyBench subset under the explicit image-tool paradigm; the runs differ only in that they are launched as separate inference jobs rather than as a single deterministic replay. Across these five matched runs, the observed ASR ranges from 17.3% to 24.8% (mean 20.3%, sample standard deviation 3.0 pp, max–min spread 7.4 pp).

Table 7: Baseline ASR (%) across five independent runs of Qwen3-VL-8B-Instruct under the explicit image-tool (CoMT/VSP) paradigm on the 202-question MM-SafetyBench subset. Same checkpoint, prompts, sampling seed, sampling rate, and judge; the runs differ only in that they are launched as separate inference jobs. The model uses `bf16` weights and activations, which combined with GPU-level nondeterminism is sufficient to drive this run-to-run spread.

Run	1	2	3	4	5	Mean	Std
ASR (%)	17.33	17.82	21.78	24.75	19.80	20.30	3.05

We attribute this drift to two compounding sources of numerical nondeterminism. First, the self-deployed Qwen3-VL-8B-Instruct runs use `bf16` weights and activations, so reductions inside attention and MLP layers absorb low-bit rounding error whose realisation depends on kernel scheduling and tensor layout. Second, GPU-level nondeterminism in atomic accumulations and in batching across runs can shift logits enough to flip tie-breaking on near-threshold harmful generations. The drift is structural rather than monotonic: independent runs do not converge to a single number, but instead cluster around different stable levels, so a single point estimate from any one run under-reports the true run-level uncertainty.

This drift shapes how we report numbers. All activation-intervention sweeps (Section 6.3, Figure 5) are launched as a single batch and report ASR *relative to a within-batch zero-injection baseline*, so that across-run drift cannot be confused with the intervention effect. The cross-paradigm gaps reported in Tables 1–3 are roughly 10–25 ASR points, several times larger than the 3.0 pp run-level standard deviation, so the qualitative ranking of paradigms is not at risk from this variation. We do not, however, claim formal statistical significance for any individual ASR cell: each table entry is a single-run point estimate, not a confidence interval over independent runs.

## F Proof of the Safety-Projection Result

*Proof of Theorem 1.* Let the safety score be  $S(z) = u^\top h(z)$  and let explicit image-tool interaction induce a residual shift  $v_{tool}$  with strength  $\alpha \geq 0$ , so that

$$h_{tool}(z) = h(z) + \alpha v_{tool}, \quad S_{tool}(z) = S(z) + \alpha u^\top v_{tool}.$$

Let  $\delta = u^\top v_{tool} > 0$  denote the safety-score increase per unit intervention strength. Under the threshold rule, the jailbreak event at strength  $\alpha$  is

$$E_\alpha = \{z : S(z) + \alpha\delta < \tau\} = \{z : S(z) < \tau - \alpha\delta\}.$$

For any  $\alpha_2 > \alpha_1 \geq 0$ , we have

$$\tau - \alpha_2\delta < \tau - \alpha_1\delta,$$

and therefore

$$E_{\alpha_2} \subseteq E_{\alpha_1}.$$

Taking probability under  $\mathcal{D}_{\text{adv}}$  gives

$$\mathcal{R}(\alpha_2) = \Pr(E_{\alpha_2}) \leq \Pr(E_{\alpha_1}) = \mathcal{R}(\alpha_1),$$

so  $\mathcal{R}(\alpha)$  is non-increasing in  $\alpha$ . The difference is

$$\mathcal{R}(\alpha_1) - \mathcal{R}(\alpha_2) = \Pr[\tau - \alpha_2 \delta \leq S(z) < \tau - \alpha_1 \delta].$$

Thus the decrease is strict exactly when the adversarial distribution has nonzero mass in the score band crossed by the shift. This proves the theorem.  $\square$

**Smooth-link variant.** The same monotonicity holds if unsafe probability is modeled as a smooth decreasing function of the safety score:

$$p_{\text{unsafe}}(z; \alpha) = \sigma(\beta(\tau - S(z) - \alpha u^\top v_{\text{tool}})),$$

where  $\sigma$  is the logistic function or any differentiable increasing link,  $\beta > 0$  controls boundary sharpness, and  $\tau$  is the operating threshold. The expected jailbreak rate under adversarial inputs is

$$\mathcal{R}_{\text{smooth}}(\alpha) = \mathbb{E}_{z \sim \mathcal{D}_{\text{adv}}} [\sigma(\beta(\tau - S(z) - \alpha u^\top v_{\text{tool}}))].$$

Differentiating with respect to  $\alpha$  gives

$$\frac{d\mathcal{R}_{\text{smooth}}(\alpha)}{d\alpha} = \mathbb{E}_{z \sim \mathcal{D}_{\text{adv}}} [\sigma'(\beta(\tau - S(z) - \alpha u^\top v_{\text{tool}})) \cdot (-\beta u^\top v_{\text{tool}})].$$

Because  $\sigma'(\cdot) > 0$  on the non-saturated range,  $\beta > 0$ , and  $u^\top v_{\text{tool}} > 0$ , the integrand is negative wherever the sample lies in that range. If the adversarial distribution has nonzero mass in the non-saturated region of the readout, then  $d\mathcal{R}_{\text{smooth}}(\alpha)/d\alpha < 0$ .

This result is intentionally local: if all adversarial examples are already far from the decision boundary, a finite residual shift may not change the observed binary ASR. The boundary diagnostics in Figure 6 check the relevant empirical condition by showing that the learned readout has nontrivial mass near its operating threshold.